Using time delay in the nonlinear oscillations of magnetic levitation for simultaneous energy harvesting and vibration suppression

Peyman Firoozy , Michael I Friswell , Qingbin Gao

PII: S0020-7403(19)30339-X
DOI: https://doi.org/10.1016/j.ijmecsci.2019.105098
Reference: MS 105098

To appear in: *International Journal of Mechanical Sciences*

Received date: 28 January 2019
Revised date: 11 July 2019
Accepted date: 23 August 2019

Please cite this article as: Peyman Firoozy , Michael I Friswell , Qingbin Gao , Using time delay in the nonlinear oscillations of magnetic levitation for simultaneous energy harvesting and vibration suppression, *International Journal of Mechanical Sciences* (2019), doi: https://doi.org/10.1016/j.ijmecsci.2019.105098

Highlights

- Theoretical model is developed to study nonlinear oscillations of magnetic levitation in the presence of time delay for vibration suppression and energy harvesting.
- The effects of the main parameters of the system, such as time delay parameters, distance between magnets, and external resistance load, is studied.
- In order to summarize the electrical and mechanical behaviors of the system, the Perfection Rate (PR) is used.
- The presence of the time delay and choosing a point from the region of multiple periodic solutions enhances the output power and suppresses higher levels of vibration.

Using time delay in the nonlinear oscillations of magnetic levitation for simultaneous energy harvesting and vibration suppression

Peyman Firoozy[1], Michael I Friswell[2*], Qingbin Gao[3]

Abstract

In this paper, the nonlinear oscillations of magnetic levitation in the presence of a time delay is investigated, with the purpose of simultaneous energy harvesting and vibration suppression. To harvest energy, a coil with seven layers of 36 gauge wire wound around the outer casing is utilized. Although the proposed control feedback consumes some power, the results show the harvestable power can be much larger than the consumed power, which makes the proposed concept feasible. The first-order perturbation method is utilized to examine the possibility of energy harvesting and vibration suppression for different selections of the delay parameters, the distances between the magnets and the external load resistances. In addition, the stability map of the time-delayed control is analytically determined. The influence of the time delay parameters chosen from Single Periodic Solutions (SPS) and Multiple Periodic Solutions (MPS) on the vibration and power amplitudes is studied. It is shown that a point chosen from the MPS region enables the system to harvest power over a broad range of excitation frequencies. Also, the effect of the distance between the magnets on the frequency response of the system is examined. In addition, to select the optimum value for the distance between the magnets for different values of the time delay parameters, a parameter called the Perfection Rate (PR), which reflects both the electrical and mechanical behavior of the system, is used. Finally, it is shown that the presence of the time delay and a point chosen from the MPS region enables the system to harvest more power over a broad range of excitation frequency and to suppress higher levels of vibration, than for a point chosen from the SPS region and without time delay.

Key words: Time delay, Broadband energy harvesting, Vibration suppression, Magnetic levitation

1. Introduction

In recent decades, harvesting environmental wasteful energies and converting them into useful electrical energies have attracted many researchers. This idea originated from the requirement to power small electronic sensors with no need of replacement batteries, especially for less accessible places. A variety of ambient energy sources such as solar, thermal, human motions and mechanical vibrations have been studied as additional energy suppliers [1, 2].

* Corresponding author
E-mail addresses: peymanfiroozy@gmail.com (P. Firoozy), m.i.friswell@swansea.ac.uk (M.I. Friswell), gaoqingbin@gmail.com (Q. Gao)
1.Department of Mechanical Engineering, Tarbiat Modares University, Tehran, Iran.
2.College of Engineering, Swansea University, Swansea, UK.
3. Department of Mechanical Engineering, The University of Alabama, Tuscaloosa, USA.

Among these alternative sources, mechanical vibrations became a prominent research direction, because of its abundance, and potential technical challenges [3-5]. A variety of methods have been proposed to convert ambient mechanical vibrations into useful electrical power such as electromagnetic [6, 7], electrostatic [8, 9], piezoelectric [10-13] and magentostrictive [4, 14]. The main problem with most energy harvesters reported in the literature is that they harvest the maximum power when the system is excited at resonance. However, a significant drop in the output power happens when the excitation frequency deviates from the resonance frequency [15]. There are many studies on the tuning of the vibration characteristics of an energy harvester by adjusting the resonance frequency including, but not limited to, adding masses [16], increasing mechanical preloads [17], and varying the geometrical parameters of the structure [18]. For all of these studies, the excitation frequency is supposed to be close to the resonance frequency. Nonlinearity features have been considered to improve the output power capability by broadening the bandwidth of the harvester [19-22]. A variety of investigations into broadband vibration energy harvesters with nonlinear monostable [23-26], bistable [27-33], and tristable [34-36] characteristics have been performed. Through experiments and simulations, Tang and Yang [37] verified the benefits of harvesting energy from the dynamics of a magnetic oscillator.

In recent decades, specific attention has been given to delay-coupled systems. It is apparent that time delay is unavoidable in active control systems since it takes time to measure, process, compute and transmit signals. At first, time delay was assumed to be an undesired feature in active control problems due to the possibility that it might cause instability of the system. More recently, researchers have considered time delay as a control parameter [38, 39]. The influence of time delayed control on quasi-zero-stiffness vibration isolators and some nonlinear isolators were investigated [40-43]. Chen et al. [43] proposed a cubic displacement feedback with time delay to improve the isolation performance of high-static-low-dynamic stiffness (HSLDS) vibration isolators. The authors concluded that time delayed feedback control performed as a damping force and the controlled HSLDS vibration isolator outperformed the passive counterpart. Liu and Liu [44, 45] designed a tunable electromagnetic vibration absorber and time delayed control was introduced to widen the operation range. Zhao and Xu [46] proposed time delayed feedback control for nonlinear absorbers with a parametrically excited pendulum. The results indicate a significant decrease by over half in the vertical vibration displacement compared to the nonlinear vibration absorber without delayed feedback control. Wang and Xu [47] proposed a vibration absorber with time-delayed feedback control to suppress vibration of the primary system under excitation with changing frequencies.

Furthermore, using time delay in vibration-based energy harvesting can have a beneficial effect on the energy harvesting performance [48]. Ghouli et al. [49] studied quasiperiodic vibration-based energy harvesting in a forced nonlinear harvester device subjected to a harmonic base excitation in which time delay was inherently present. They concluded that the proposed energy harvester, with optimal values of the time delay, can extract more power over a broad range of frequencies away from the resonance. Belhaq and Hamdi [48] studied quasiperiodic

vibration-based energy harvesting in a delayed van der Pol oscillator with time-varying delays coupled to an electromagnetic energy harvesting device. They assumed that the vibration source of the proposed device is due to self-excitation. The authors concluded that the proposed energy harvester is capable of harvesting more power over a broad range of excitation frequencies. Ghouli et al. [50] added a time delay into the electromagnetic energy harvester studied in [48]. They concluded that the introduced time delay in the electrical circuit is able to control and optimize the energy harvesting performance. Also, the authors reported that the maximum vibration amplitude does not yield the maximum output power. Studying vibration based energy harvesting in a delayed energy harvester device can be useful in certain applications for which a delayed state feedback is present in the mechanical subsystem of the harvester. For example, in milling and turning operations the time delay inherently occurs in the process and the time delay is not considered as an additional input power of the harvester [51-53]. Kammer and Olgac [54, 55] proposed the idea of using time delay in the feedback control. The authors theoretically and experimentally showed that the idea significantly increases the energy harvesting capacity of vibration absorbers by sensitizing the structure with the use of the feedback control law. They also studied delayed feedback control in piezoelectric networks [54]. The time delay can also be used to extend the dynamic range of an energy harvester with nonlinear damping [55] demonstrating that it can substantially enhance the energy harvester capacity. However, in such applications the time delay is presented as an input power, and the problem of the energy balance between the produced and consumed powers should be examined [55].

Based on the literature, utilizing nonlinear properties in an energy harvesting system can significantly shift the resonance frequency away from the linear resonance, and thus enable the system to harvest more power over an extended range of frequencies. In addition, research on the nonlinear system that can harvest energy and simultaneously suppress undesired vibrations using time delayed control is missing in the literature. We propose a concept to enhance the energy harvesting capacity from mechanical vibrations using a delayed feedback tuning mechanism. We take advantage of the magnetic levitation between two fixed magnets and introduce a time delay in the system feedback to harvest more power over a broad range of excitation frequencies. First, we calculate the power required for the control force to confirm that the power required by the feedback mechanism is significantly less than the harvester power. Second, we plot the stability map of the system in the domain of the delay parameters to study the influence of the different parameters on the harvester power. To select the optimum value for the distance between magnets for different time delays, the perfection rate (PR) parameter is introduced. Finally, the effect of the time delay parameters and the external load resistance on the frequency response function of the vibration and the net generated power are studied.

a

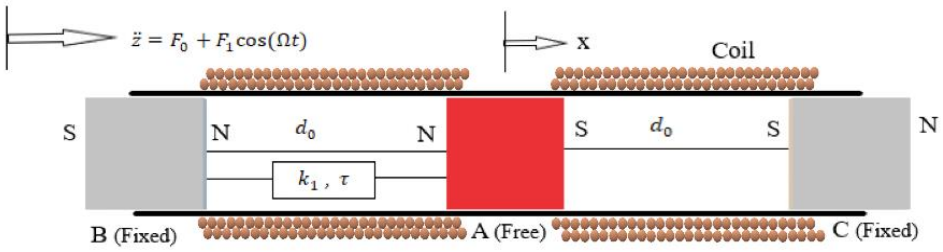

b

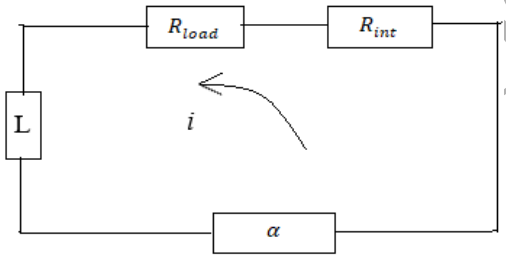

Fig. 1 **(a)** A schematic of the energy harvester consists of two fixed magnets (B and C), a free magnet (A) and mechanical feedback control including the time delay and gain (τ, k_1) and harmonic base acceleration, $\ddot{z}(t)$, **(b)** the electrical circuit diagram (R_{load} R_{int}, and L represent the resistances of the external and internal loads and the inductance of the coil, respectively).

2. Magnetic repulsion force

Figure 1(a) shows the studied energy harvesting device which consists of two fixed magnets and one free magnet, and a mechanical feedback control including a time delay defined by the parameters (k_1, τ). The corresponding electrical circuit diagram for energy harvesting is presented in Fig. 1(b). To mathematically formulate the energy harvesting equations of motion, we first obtain the magnetic repulsion force by assuming that the magnets are modeled as point dipoles. Since the forces between two magnetic dipoles are a function of spatial derivatives of their magnetic fields, it is difficult to determine the direction and magnitude of these forces. Therefore, in the current study, the dipole magnets are assumed to be either parallel or perpendicular to the separation vector between the dipoles. Yung et al. [56] proposed that different magnet arrangements result in different potential energies of the magnetic field, and the magnetic field generated by dipole A at the location B, or $\boldsymbol{B}_{AB}$, and at the location C, or $\boldsymbol{B}_{AC}$, respectively, is given by [20]

$$\boldsymbol{B}_{AB} = -\frac{\mu_0}{4\pi}\nabla\left(\frac{\vec{\boldsymbol{\mu}}_{\boldsymbol{A}}.\vec{\boldsymbol{r}}_{\boldsymbol{AB}}}{\|\vec{\boldsymbol{r}}_{\boldsymbol{AB}}\|_{\boldsymbol{2}}^{\boldsymbol{3}}}\right) \quad (1)$$

$$\boldsymbol{B}_{AC} = -\frac{\mu_0}{4\pi}\nabla\left(\frac{\vec{\boldsymbol{\mu}}_{\boldsymbol{A}}.\vec{\boldsymbol{r}}_{\boldsymbol{AC}}}{\|\vec{\boldsymbol{r}}_{\boldsymbol{AC}}\|_{\boldsymbol{2}}^{\boldsymbol{3}}}\right) \quad (2)$$

where $\|.\|_{\boldsymbol{2}}$, ∇, and $\mu_0 = 4\pi \times 10^{-7}\mathrm{H/m}$ denote the Euclidean norm, the vector gradient operator, and the magnetic constant, respectively. Also, $\vec{\boldsymbol{r}}_{\boldsymbol{AB}}$ and $\vec{\boldsymbol{r}}_{\boldsymbol{AC}}$ denote the vectors from the center of magnet A to the centers of magnets B and C, respectively. In addition, $\vec{\boldsymbol{\mu}}_{\boldsymbol{A}}$, $\vec{\boldsymbol{\mu}}_{\boldsymbol{B}}$ and $\vec{\boldsymbol{\mu}}_{\boldsymbol{C}}$ are the magnetic moment vectors of magnets A, B, and C, respectively, and can be written as [33]

$$\boldsymbol{\mu} = \boldsymbol{M}V \quad (3)$$

where $\boldsymbol{M}$ is the magnetization vector which represents the sum of all of the microscopic magnetic moments within a ferromagnetic material, and V is the volume of the magnet. The corresponding potential energies of the magnetic fields presented in Eqs. (1) and (2) are given by [33]

$$U_{AB} = -\boldsymbol{B}_{AB}.\vec{\boldsymbol{\mu}}_{\boldsymbol{B}} \quad (4)$$

$$U_{AC} = -\boldsymbol{B}_{AC}.\vec{\boldsymbol{\mu}}_{\boldsymbol{C}} \quad (5)$$

By substituting Eqs. (1), (2) and (3) into Eqs. (4) and (5) and assuming that $M_A = M_B = M_C = 0.955 \times 10^6\mathrm{A/m}$, and $V_A = V_B = V_C = 4\pi\ \mathrm{mm}^3$ one can obtain the following potential energies

$$U_{AB} = \frac{\mu_0 M^2 V^2}{2\pi}\left[\frac{1}{(d_0 - x)^3}\right] \quad (4)$$

$$U_{AC} = \frac{\mu_0 M^2 V^2}{2\pi}\left[\frac{1}{(d_0 + x)^3}\right] \quad (5)$$

where d_0 is the separation distance between the two magnets and x is the displacement of the center magnet at time t. The forces exerted by dipole A upon dipole B, or F_{AB}, and upon dipole C, or F_{AC}, can be derived from the potential energies as [33, 56]

$$F_{AB} = \nabla U_{AB} \quad (6)$$

$$F_{AC} = \nabla U_{AC} \quad (7)$$

By substituting Eqs. (4) and (5) into Eqs. (6) and (7) and assuming $F_m = F_{AC} - F_{AB}$ as the sum of forces exerted on magnet A by magnets B and C, one may obtain

$$F_m = -\frac{3\mu_0 M^2 V^2}{2\pi}\left[\frac{1}{(d_0 + x)^4} - \frac{1}{(d_0 - x)^4}\right] \quad (8)$$

where $x = 0$ is the equilibrium position of the energy harvester and can be calculated from Eq. (8). In the following part, we expand the expression of the magnetic force as a Taylor series about the equilibrium point, i.e. $x = 0$, and the higher orders are neglected

$$F_m = \frac{12\mu_0 M^2 V^2}{\pi}\left[\frac{1}{{d_0}^5}x + \frac{5}{{d_0}^7}x^3\right] \tag{9}$$

For the sake of simplicity, we define the following constants

$$k = \frac{12\mu_0 M^2 V^2}{\pi {d_0}^5} \tag{10}$$

$$k_3 = \frac{60\mu_0 M^2 V^2}{\pi {d_0}^7} \tag{11}$$

Substituting Eqs. (10) and (11) into Eq. (9), we obtain

$$F_m = kx + k_3 x^3 \tag{12}$$

Using these expressions for the magnetic force, we will proceed to the derivation of the governing equations in the next section.

3. Governing equations and periodic energy harvesting

To harvest energy, a coil with seven layers of 36 gauge wire wound around the outer casing is utilized, as described in [15] and shown in Fig. 1(a). Also, it is assumed that the structure is excited with harmonic base excitation $\ddot{z} = F_0 + F_1\cos(\Omega t)$, where F_0 is the unmodulated amplitude and F_1 and Ω are the amplitude and frequency of the base excitation, respectively. In order to obtain the equation for the electrical circuit, we apply Kirchoff's voltage law to the electrical circuit shown in Fig. 1(b). Thus [15]

$$L\frac{di}{dt} + R_{eq}i - \alpha(\dot{x} - \dot{z}) = 0 \tag{13}$$

where i and $\frac{di}{dt}$ are the current and derivative of the current with respect to time, t, respectively, and have been used instead of the electric charge q ($i = \dot{q}$). Also, $R_{eq} = R_{load} + R_{int}$ is the equivalent load resistance which is a combination of R_{load}, which represents the resistance of the external load, and R_{int}, which denotes the internal resistance of the coil. L is the inductance of the harvesting coil and α is the electromechanical coupling coefficient and is commonly expressed as $\alpha = NBl$, where N, B, and l are the number of coil turns, the average magnetic field strength, and the coil length, respectively. By using Newton's second law, and introducing $y = x - z$ as a new variable one may obtain the following electromechanical equation

$$m\ddot{y} + c_m\dot{y} + ky + k_3y^3 - \alpha i = k_1y(t-\tau) + m(F_0 + F_1\cos(\Omega t)) \quad (14)$$

where m is the mass of the magnet, c_m is the mechanical damping coefficient, k_1 is the gain of the delay and τ is the time delay. We introduce the following non-dimensional parameters: $2\xi\omega = \frac{c_m}{m}$, $\beta = \frac{k_3}{m}$, $\gamma_2 = \frac{R_{eq}}{L}$, $\gamma_3 = \frac{\alpha}{L}$, $\hat{k}_1 = \frac{k_1}{m}$ where $\omega = \sqrt{\frac{k}{m}}$ is the natural frequency of the energy harvester. Next, we introduce a bookkeeping parameter ε and scale the following parameters: $2\varepsilon\mu = 2\xi\omega$, $\varepsilon\hat{\beta} = \beta$, $F_1 = 2\varepsilon\hat{F}_1$, $\gamma_1 = \varepsilon\gamma_1$ where $\gamma_1 = \frac{\alpha}{m}$, and $\hat{k}_1 = \varepsilon\hat{k}_1$. By using the alternative non-dimensional parameters and reordering the parameters in Eqs. (13) and (14) we obtain the following equations

$$\ddot{y} + 2\varepsilon\mu\dot{y} + \omega^2y + \varepsilon\hat{\beta}y^3 - \varepsilon\gamma_1 i = \varepsilon\hat{k}_1y(t-\tau) + F_0 + 2\varepsilon\hat{F}_1\cos(\Omega t) \quad (15)$$

$$\frac{di}{dt} + \gamma_2 i = -\gamma_3\dot{y} \quad (16)$$

Next, we solve the described equations analytically with the assistance of the multiple scale time method [57]. A solution to Eqs. (15) and (16) up to the second order approximation is sought in the form

$$y(t) = y_0(T_0, T_1, T_2) + \varepsilon y_1(T_0, T_1, T_2) + \varepsilon^2 y_2(T_0, T_1, T_2) + O(\varepsilon^3) \quad (17)$$

$$i(t) = i_0(T_0, T_1, T_2) + \varepsilon i_1(T_0, T_1, T_2) + \varepsilon^2 i_2(T_0, T_1, T_2) + O(\varepsilon^3) \quad (18)$$

$$y(t-\tau) = y_\tau = y_{0\tau}(T_0, T_1, T_2) + \varepsilon y_{1\tau}(T_0, T_1, T_2) + \varepsilon^2 y_{2\tau}(T_0, T_1, T_2) + O(\varepsilon^3) \quad (19)$$

where $T_0 = t$ is the fast time scale and two other slow time scales are defined as $T_1 = \varepsilon t$, $T_2 = \varepsilon^2 t$, and $O(\varepsilon^3)$ indicates the higher order terms. We omit the circumflex in the following equations for the sake of notational simplicity. The time derivatives in terms of variables T_i are formulated as [58]

$$\frac{d}{dt} = D_0 + \varepsilon D_1 + \varepsilon^2 D_2 + O(\varepsilon^3) \quad (20)$$

$$\frac{d^2}{dt^2} = {D_0}^2 + \varepsilon^2({D_1}^2 + 2D_0D_2) + 2\varepsilon D_0D_1 + O(\varepsilon^3) \quad (21)$$

where $D_i^j = \frac{\partial^j}{\partial^j T_i}$. Substituting Eqs. (17)-(21) into Eqs. (15) and (16) we obtain the following set of equations in the successive perturbation order:

$${D_0}^2y_0 + \omega^2y_0 = F_0 \quad (22)$$

$$D_0i_0 + \gamma_2 i_0 + \gamma_3 D_0y_0 = 0 \quad (23)$$

$${D_0}^2y_1 + \omega^2y_1 = -2D_0D_1y_0 - \beta{y_0}^3 - 2\mu D_0y_0 + \gamma_1 i_0 + k_1 i_{0\tau} + 2F_1\cos(\Omega t) \quad (24)$$

$$D_0 i_1 + \gamma_2 i_1 = -\gamma_3 D_0 y_1 - \gamma_3 D_1 y_0 - D_1 i_0 \tag{25}$$

$$D_0{}^2 y_2 + \omega^2 y_2 = -D_1{}^2 y_0 - 2D_0 D_2 y_0 - 2D_0 D_1 y_1 - 2\mu D_1 y_0 - 2\mu D_0 y_1 - 3\beta y_1 y_0{}^2 + \gamma_1 i_1 + k_1 i_{1\tau} \tag{26}$$

$$D_0 i_2 + \gamma_2 i_2 = -\gamma_3 D_0 y_2 - \gamma_3 D_1 y_1 - \gamma_3 D_2 y_0 - D_2 i_0 - D_1 i_1 \tag{27}$$

The solution of Eqs. (22) and (23) is expressed in complex form as

$$y_0(T_0, T_1, T_2) = A(T_1, T_2) e^{i\omega T_0} + \bar{A}(T_1, T_2) e^{-i\omega T_0} \tag{28}$$

$$i_0(T_0, T_1, T_2) = -\frac{\gamma_3 i\omega A(T_1, T_2)}{y_2 + i\omega} e^{i\omega T_0} + \frac{\gamma_3 i\omega A(T_1, T_2)}{y_2 - i\omega} e^{-i\omega T_0} \tag{29}$$

where $A(T_1, T_2)$ and $\bar{A}(T_1, T_2)$ are unknown complex conjugate functions. Substituting Eqs. (28) and (29) into Eqs. (24) and (25) yields

$$D_0{}^2 y_1 + \omega^2 y_1 = \left[-2i\omega(A' + \mu A) - \beta\left(3A^2\bar{A} + \frac{3A{F_0}^2}{\omega^4}\right) - \frac{\gamma_1\gamma_3 i\omega A}{\gamma_2 + i\omega} + k_1 A e^{-i\omega\tau}\right] e^{i\omega T_0} - \beta\left[A^3 e^{3i\omega T_0} + \frac{3F_0}{\omega^2} A^2 \bar{A} e^{2i\omega T_0} + \bar{A}^3 e^{-3i\omega T_0} + \frac{{F_0}^2}{\omega^2}\left(3A\bar{A} + \frac{{F_0}^2}{2\omega^4}\right)\right] + 2F_1 \cos(\Omega t) + CC \tag{30}$$

where the prime denotes the derivative with respect to T_1 and CC denotes the complex conjugate of the terms on the right-hand side.

We now analyze and obtain the frequency responses of the energy harvester close to the primary resonance, i.e. $\Omega = \omega + \varepsilon\sigma$, where σ is called a detuning parameter and acts to describe the proximity of Ω to ω. After substituting the introduced detuning parameter into Eq. (30) and also eliminating the secular terms one can obtain

$$-2i\omega(A' + \mu A) - \beta\left(3A^2\bar{A} + \frac{3A{F_0}^2}{\omega^4}\right) - \frac{\gamma_1\gamma_3 i\omega A}{\gamma_2 + i\omega} + k_1 A e^{-i\omega\tau} + F_1 e^{i\sigma T_2} = 0 \tag{31}$$

Eliminating from Eq. (30) the secular generating terms we have the following solutions

$$y_1(T_0, T_1, T_2) = \frac{\beta A^3}{8\omega^2} e^{3i\omega T_0} + \frac{\beta\bar{A}^3}{8\omega^2} e^{-3i\omega T_0} + \frac{\beta F_0 \bar{A} A^2}{\omega^4} e^{2i\omega T_0} - \frac{\beta F_0}{\omega^4}\left(3A\bar{A} + \frac{F_0}{2\omega^4}\right) \tag{32}$$

$$i_1(T_0, T_1, T_2) = 0 \tag{33}$$

Substituting $A = \frac{1}{2} a e^{i\theta}$, where a and θ are the amplitude and the phase of the modulation, respectively, into Eq. (31) and then separating the obtained equation into the real and imaginary components, one may obtain the two modulation equations as

$$\frac{da}{dt} = -\mu a - \frac{\gamma_1\gamma_2\gamma_3}{2({\gamma_2}^2+\omega^2)}a - \frac{1}{2\omega}k_1\, a\sin(\omega\tau) + \frac{F_1}{\omega}\sin\varphi \tag{34}$$

$$a\frac{d\varphi}{dt} = a\sigma - \frac{3}{8\omega}\beta\left(a^3 + 4a\frac{{F_0}^2}{\omega^4}\right) - \frac{\gamma_1\gamma_3\omega}{2({\gamma_2}^2+\omega^2)}a + \frac{1}{2\omega}k_1\, a\cos(\omega\tau) + \frac{F_1}{\omega}\cos\varphi \tag{35}$$

where $\varphi = \sigma T_2 - \theta$.

By setting $\frac{da}{dt} = 0$ and $a\frac{d\varphi}{dt} = 0$ in the above equations we obtain the steady-state responses. Eliminating the phase in the obtained results lead to the following algebraic equation in a

$${C_3}^2a^6 + 2C_2C_3a^4 + \left({C_1}^2 + {C_2}^2\right)a^2 - f^2 = 0 \tag{36}$$

where $f = \frac{F_1}{\omega}$ and C_i are given in Appendix A.

The solution up to the first order can be written as $y_0(T_0, T_1, T_2) = a\cos(\omega t + \theta)$ and $i_0(T_0, T_1, T_2) = I\cos(\omega t + \theta - \arctan\frac{\gamma_2}{\omega})$ where I is the current amplitude and defined as

$$I = \frac{\gamma_3\omega}{\sqrt{{\gamma_2}^2+\omega^2}}a \tag{37}$$

One can obtain the average power as

$$P_{av} = \frac{1}{2}\left(\frac{\gamma_2{\gamma_3}^2\omega^2}{{\gamma_2}^2+\omega^2}\right)a^2 \tag{38}$$

where a is obtained from Eq. (36).

To analyze the stability and instability of the periodic responses we next linearize the steady-state solutions with respect to a and φ. For this, the Jacobian Matrix for Eqs. (34) and (35) in terms of the physical parameters for the energy harvester is defined as

$$J = \begin{bmatrix} -\xi\omega - \frac{\gamma_1\gamma_2\gamma_3}{2({\gamma_2}^2+\omega^2)} - \frac{1}{2\omega}k_1\sin(\omega\tau) & \frac{F_1}{2\omega}\cos\varphi \\ -\frac{6\beta}{8\omega}a - \frac{\gamma_1\gamma_3\omega}{2({\gamma_2}^2+\omega^2)} + \frac{1}{2\omega}k_1\cos(\omega\tau) + \frac{F_1}{2\omega a^2}cos\varphi & -\frac{F_1}{2a\omega}\sin\varphi \end{bmatrix} \tag{39}$$

The system response is stable if all the real parts of the eigenvalues of the Jacobian Matrix, Eq. (39), are less than zero, otherwise the system response will be unstable.

4. Energy balance of the system

The studied energy harvester, shown in Fig. 1, consists of a delayed proportional feedback control that requires an actuator to provide the force. Thus the energy inventory of the proposed

energy harvester should be carefully assessed [55]. For this, we assume that a purely harmonic base motion of frequency Ω yields the following frequency response

$$x(t) = X\cos(\Omega t + \varphi) \tag{40}$$

where X and φ are the amplitude and phase, respectively. Then we assume that $y = x - z$, which is the relative motion between magnet A and base displacement, is

$$y(t) = Y\cos(\Omega t + \psi) \tag{41}$$

where Y and ψ are the amplitude and phase, respectively.

Now we obtain the power harvested by the transducer as

$$P_{gen} = \alpha\dot{y}^2 = \alpha\Omega^2 Y^2 \sin^2(\Omega t + \psi) \tag{42}$$

and the corresponding energy generated per cycle is

$$E_{gen} = \alpha\Omega^2 Y^2 \int_0^T \sin^2(\Omega t + \psi)\, dt = \frac{\alpha\Omega^2 Y^2 \pi}{\Omega} \tag{43}$$

where $T = 2\pi/\Omega$ denotes the period of oscillation. One may obtain the average power per cycle as follows

$$P_{gen}^{av} = \frac{\alpha\Omega^2 Y^2}{2} \tag{44}$$

Next, we obtain the power required for the active control as

$$P_{act} = k_1 x(t-\tau)\dot{y}(t) = -k_1 YX\Omega \sin(\Omega t + \psi)\cos(\Omega t + \varphi - \Omega\tau) \tag{45}$$

Following the same procedure, one can obtain the average power consumption per cycle as

$$P_{act}^{av} = \frac{k_1 YX\Omega \sin(\Omega\tau + \psi - \varphi)}{2} \tag{46}$$

In next section, we use Eqs. (44) and (46) to confirm that the harvestable power can be much larger than the consumed power which makes the proposed concept feasible. Then, by using Eqs. (36) and (38), we study the influence of the different parameters on the scavenged power and the vibration amplitude.

5. Results and Discussions

Figure 2 shows the variation of the generated, consumed and harvested (generated minus consumed) powers with respect to the normalized excitation frequency for the delay parameters $k_1 = 4$ and $\tau = 0.4131$. As can be seen, the potential harvested power increases monotonically

as the excitation frequency increases. In addition, Fig. 2 shows that the actuator power requirement is quite small and indicates the benefit of power harvesting by using a time delay in the studied system.

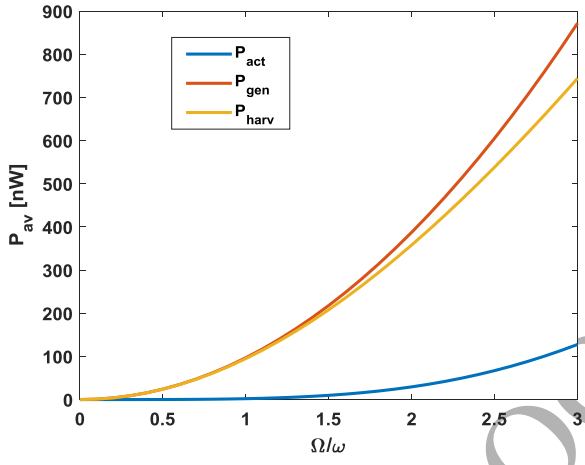

Fig. 2 Average powers vs. normalized excitation frequency for the delay parameters $k_1 = 4$ and $\tau = 0.4131$.

Next, the influence of different parameters on the system's frequency responses are presented. First, we plot the stability map of the system in the domain of the delay and its gain, i.e. τ and k_1. For this, we obtain the characteristics of the system based on the analytical solution from the first order approximation (Eqs. (34) and (35)) as

$$\lambda^2 + Tr(J)\lambda + Det(J) = 0 \tag{47}$$

where the trace $Tr(J)$ and determinant $Det(J)$ of the first order Jacobian Matrix (Eq. (38)) are obtained as

$$Tr(J) = 2\left(\frac{C_4}{2\omega}\right)^2 \tag{48}$$

$$Det(J) = \left(\frac{C_4}{2\omega}\right)^2 + C_5 C_6 \tag{49}$$

where $C_{i=4,5,6}$ constants are defined as

$$C_4 = 2\xi\omega^2 + \frac{\gamma_1\gamma_2\gamma_3\omega}{{\gamma_2}^2 + \omega^2} + k_1 \sin(\omega\tau) \tag{50}$$

$$C_5 = \sigma - \frac{3\beta}{8\omega}\left(3a^2 + 4\frac{{F_0}^2}{\omega^4}\right) - \frac{\gamma_1\gamma_3\omega}{{\gamma_2}^2 + \omega^2}a + \frac{1}{\omega}k_1 \cos(\omega\tau)\, a \tag{51}$$

$$C_6 = \sigma - \frac{3\beta}{8\omega}\left(3a^2 + 4\frac{{F_0}^2}{\omega^4}\right) - \frac{\gamma_1\gamma_3\omega}{{\gamma_2}^2 + \omega^2}a + \frac{1}{2\omega}k_1 \cos(\omega\tau)\, a \tag{52}$$

Substituting Eqs. (50)-(52) into Eqs. (48) and (49) one can obtain $Tr(J)$ in its simplest form as

$$Tr(J) = 2\xi\omega^2 + \frac{\gamma_1\gamma_2\gamma_3\omega}{{\gamma_2}^2 + \omega^2} + k_1 \sin(\omega\tau) \tag{53}$$

Notice that $Tr(J)$ is independent of the nonlinearity and the resonance amplitude, and hence $Tr(J)$ does not depend on the excitation frequency and its amplitude. On the basis of this explanation, the regions of the Single Periodic Solutions (SPS) and the Multiple Periodic Solutions (MPS) of the original system for the arbitrarily-selected parameters $d_0 = 19.53$ mm, $m = 19.5$g, $\xi = 0.115$, $\gamma_1 = 397.4872$, $\gamma_2 = 5.9891 \times 10^3$, and $\gamma_3 = 0.0464$ are shown in Fig. 3. In the SPS region there exists a single stable periodic solution, whereas in the MPS region both stable and unstable periodic solutions exist, and in practice the system would converge to one of the stable solutions. In addition, one can obtain the critical values of the delay gain (k_{cr}) from Eq. (53) as

$$k_{cr} = \omega(2\xi\omega + \frac{\gamma_1\gamma_2\gamma_3}{{\gamma_2}^2 + \omega^2}) \tag{54}$$

According to Eqs. (53) and (54), and considering that $\sin(\omega\tau) < 1$, if $k_{cr} > k_1$ the system has stable solutions, otherwise the system response would be influenced by the time delay τ.

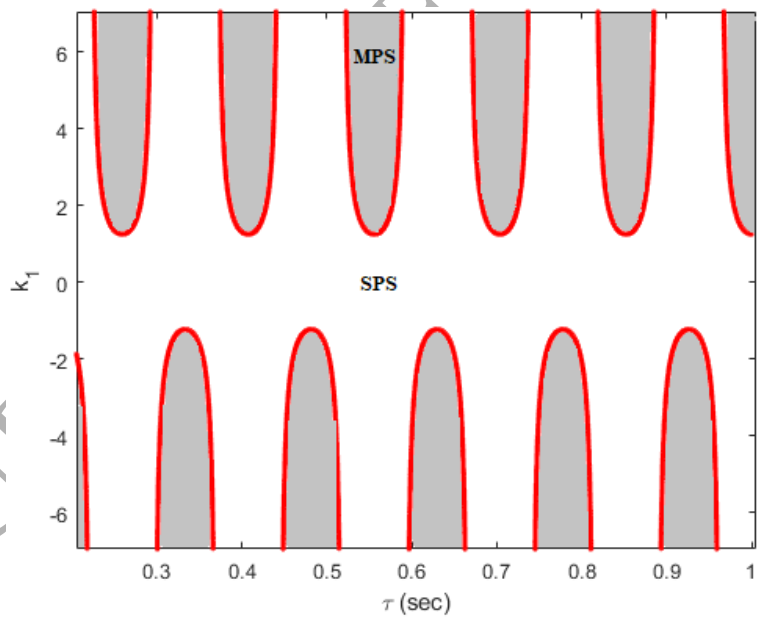

Fig. 3 Stability map of the periodic solutions in the domain (k_1, τ) for parameters $d_0 = 19.53$ mm, $m = 19.5$g, $\xi = 0.115$, $\gamma_1 = 397.4872$, $\gamma_2 = 5.9891 \times 10^3$, and $\gamma_3 = 0.0464$. SPS: Single Periodic Solution, MPS: Multiple Periodic Solution.

Next, we study the influence of several points chosen from the SPS and MPS regions in Fig. 3 on the vibration and power amplitudes. Figure 4 shows the influence of the time delay gain chosen from the MPS region (for $\tau = 0.4131$) in Fig. 3 on the frequency response of the

vibration and power amplitudes. The physical parameters are assumed to be the same as in Fig. 3. The unstable solutions are shown in red whereas the stable solutions are denoted with the colors other than red. The response exhibits a hardening spring-type behavior, and there are multiple solutions in the frequency response curves. The energy harvester response settles on either the stable or unstable branch depending on the initial conditions. Therefore, the energy harvester can experience nonlinear dynamical behaviors such as the jump phenomena and hysteresis in this region. It is seen that the vibration amplitude and power amplitude varies with different values of the time delay gain. Also, it is seen that the system has nonlinear hardening behavior for time delay gains of $k_1 = 0$ and $k_1 = 4$. Further increases in the time delay yields a system response with a linear behavior which results in a significant drop in the vibration and power amplitudes. The results highlight the key influence of the time delay gain on the system responses.

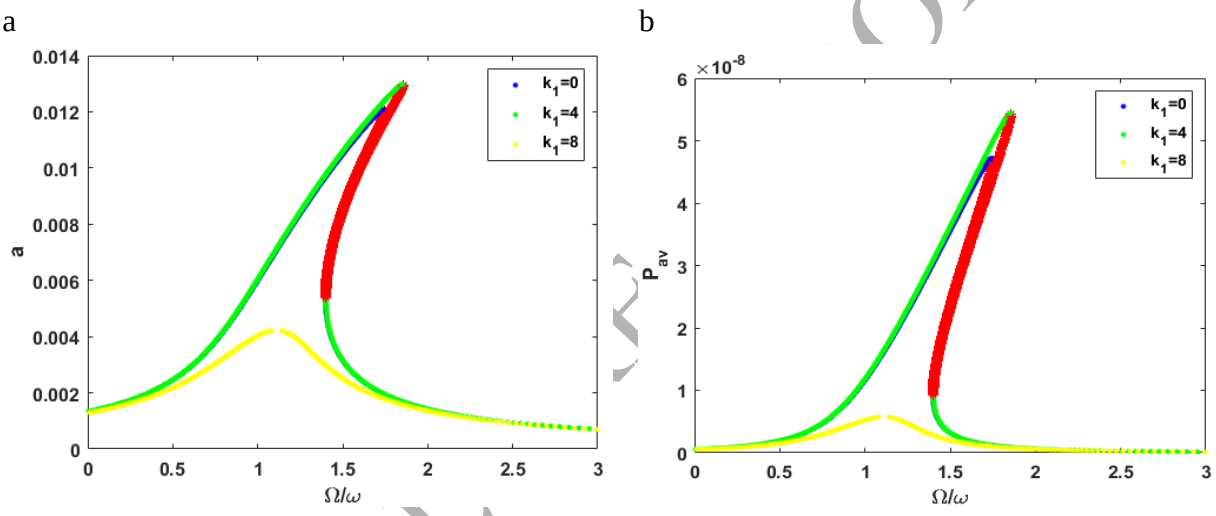

Fig. 4 Influence of the time delay gain k_1 chosen from the MPS region ($\tau = 0.4131$) on the **(a)** vibration and **(b)** power amplitudes.

a b

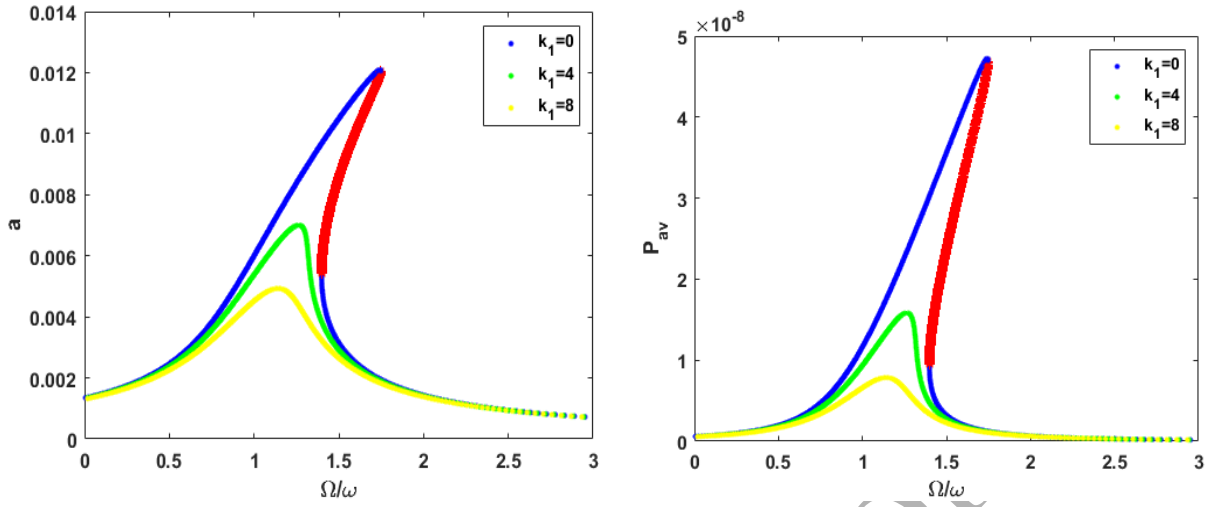

Fig. 5 Influence of the time delay gain k_1 chosen from the SPS region ($\tau = 0.75$) on the **(a)** vibration and **(b)** power amplitudes.

Figure 5 shows the influence of the different values of the time delay gains chosen from the SPS region ($\tau = 0.75$) on the vibration and power amplitudes, for similar conditions to Fig. 4. It is seen that as the time delay gain is increased the instability and hysteresis regions in the system responses disappear. In addition, the system responses are changed from a hardening behavior without time delay to a linear behavior as the time delay gain increased. Also, a significant drop in the vibration and power amplitudes is observed; the vibration amplitudes are 0.0122 and 0.007 without the time delay and with a delay gain of $k_1 = 4$, respectively, which exhibits a significant reduction of 74.3% in the vibration amplitude.

The influence of the distance between the magnets without the time delay and with a time delay chosen from the SPS and MPS regions on the vibration and power amplitudes are shown in Fig. 6. The red color indicates the unstable responses, whereas the stable responses are shown in colors other than red. It is seen that without the time delay and for small values of d_0 the system has a linear behavior. Increasing d_0 shifts the resonance frequency to the right which leads to a nonlinear hardening behavior for the system. Also, increasing d_0 results in higher vibration and power amplitudes. For example, when the distance between magnets is equal to 15 mm the vibration and power amplitudes are equal to 3.22mm and 0.0125μW, respectively, and the resonance frequency for the corresponding vibration and power amplitudes occur at a frequency ratio of 1.1. Changing d_0 from 15mm to 20mm significantly affects the system's responses. For example, the vibration and power amplitudes are now 14mm and 0.053μW, respectively, which occur at frequency ratios of 1.948 and 1.9, respectively. Comparison of the output power for $d_0 = 15\text{mm}$ and $d_0 = 20\text{mm}$ indicates a 324% increase in the scavenged power for $d_0 = 20\text{mm}$. Figure 6(c) and (d) show the vibration and power frequency responses with a time delay of $\tau = 0.75$ chosen from the SPS region for a delay gain of $k_1 = 4$. Increasing d_0 results in an increase in the vibration amplitude and interestingly a decrease in the output power. Varying d_0

from 15 mm to 20 mm changes the natural frequency of the system from 82 rad/s to 40 rad/s. Since ω appears in the average power coefficient (Eq. (38)), it affects the average power significantly and causes a decrease in the output power if d_0 is changed from 15 mm to 20 mm. Also, for this case it is seen that the system has a nonlinear hardening behavior even for the small values of d_0, in contrast to the system without a time delay which has a linear behavior as discussed earlier. Comparison of the output power between the systems with and without time delay parameters chosen from the SPS region reveals the importance of the time delay in the studied energy harvester. For example, when $d_0 = 15\text{mm}$ the output power without a time delay is 0.0125μW while it is 0.0539μW (a 331.2% increase) with a time delay. Also, the effect of the distance between magnets on the frequency response of the vibration and power amplitudes with a time delay of $\tau = 0.4131$ chosen from the MPS region for the delay gain of $k_1 = 4$ is studied in Fig. 6(e) and (f). For $d_0 = 20\text{mm}$ a significant increase in the resonance frequency occurs compared to the system without a time delay and with time delay parameters chosen from the SPS region. This enables the system to harvest more power over a broad range of excitation frequencies away from the primary resonance frequency.

a

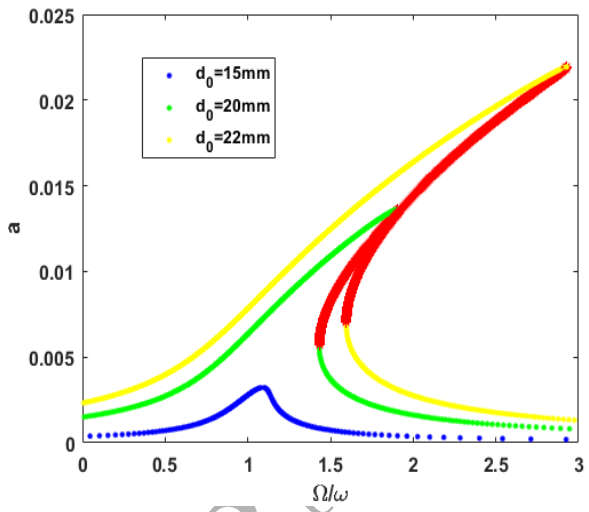

b

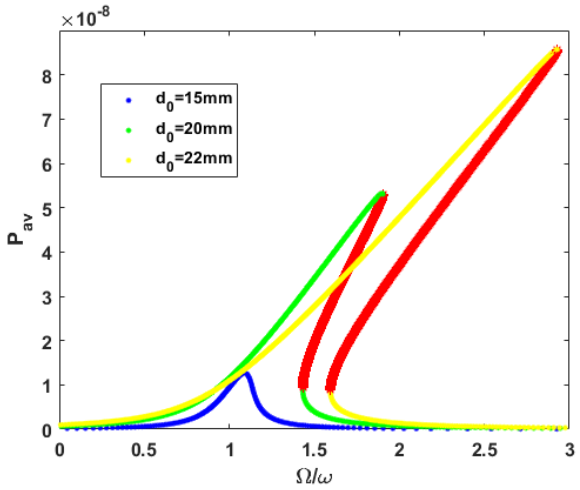

c

d

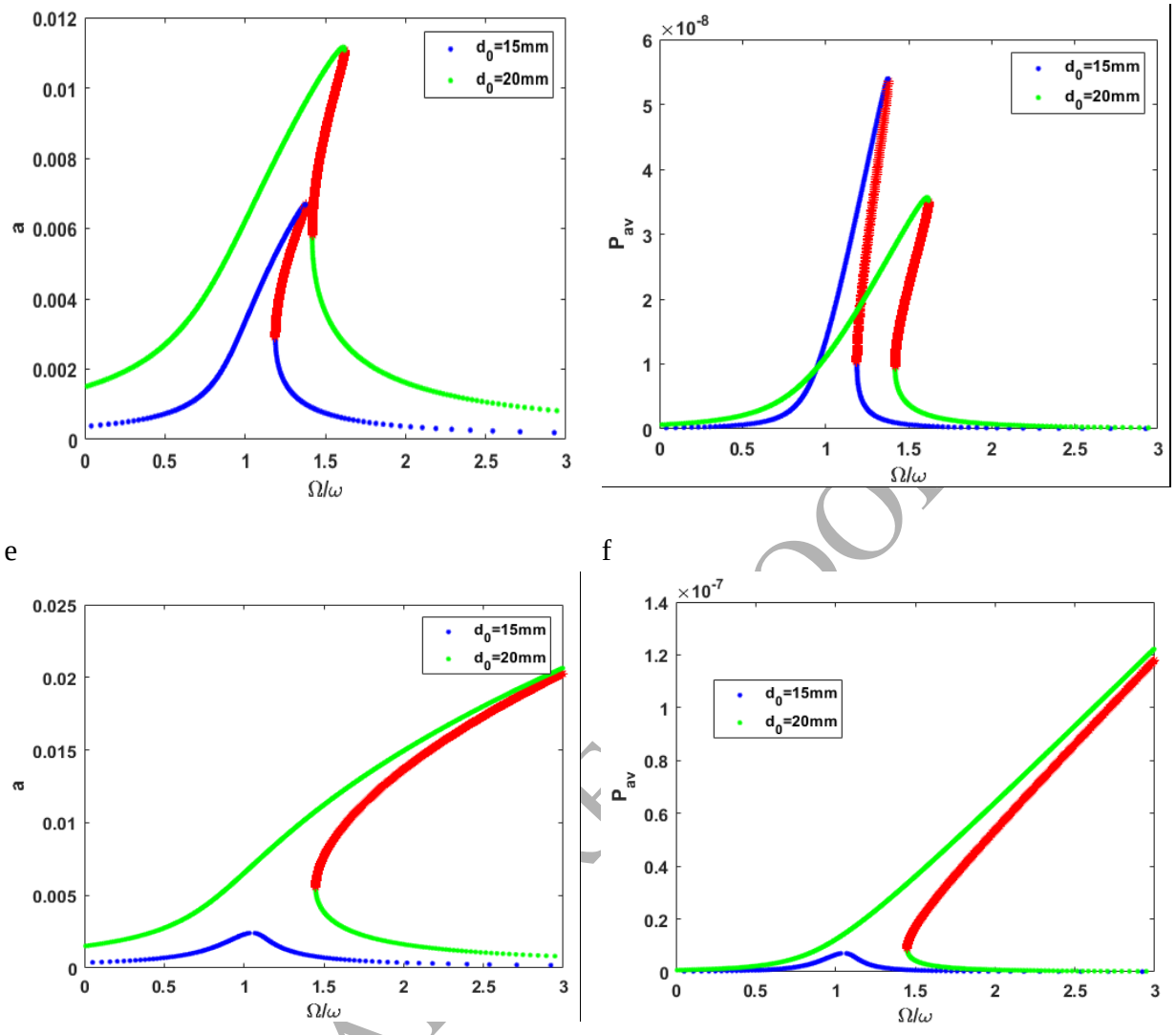

Fig. 6 Influence of the distance between the magnets d_0 on the vibration and power amplitudes: **(a, b)** without time delay, **(c, d)** with time delay $k_1 = 4$ chosen from the SPS region ($\tau = 0.75$), and **(e, f)** with time delay $k_1 = 4$ chosen from the MPS region ($\tau = 0.4131$).

Since we are trying to design a system that can maximize the harvested energy and minimize the mechanical displacement simultaneously, we define the so-called Perfection Rate (PR). The PR summarizes both electrical-based and mechanical-based performance in a variable defined as [59, 60]:

$$PR(\%) = (WF_1 \times \frac{P_{rms}}{P_{max}} + WF_2 \times \frac{a_{rms}}{a_{max}}) \times 100 \quad (55)$$

where WF_1 and WF_2 are weighting factors for the power-based and vibration-based objectives, respectively. P_{rms} and a_{rms} are the root-mean-squares of the output power and vibration,

respectively, and P_{max} and a_{max} are the maxima of the output power and vibration, respectively. The weighting factors are in the range of the zero to one and their sum is equal to one ($WF_1 + WF_2 = 1$). We select three different arbitrarily selected values for the WF_1 to show the importance of the output power or vibration. These values are selected as $WF_1 = 0.2$ (to show the importance of the vibration), $WF_1 = 0.8$ (to demonstrate the significance of the output power). Also, $WF_1 = 0.5$ entails equal importance to the output power and vibration. The best value of d_0 for the physical and electrical parameters of $F_0 = 2\,\mathrm{m/s^2}$, $F_1 = 5\,\mathrm{m/s^2}$, $R_{eq} = 188\mathrm{M\Omega}$, $\alpha = 7.751$ and $L = 167$ is shown in Table 1. The highest perfection rate occurs for $WF_1 = 0.2$, $k_1 = 4$, and $\tau = 0.4131$ when $d_0 = 15$ mm. The presence of the time delay and for the delay parameters chosen in the MPS region not only produces more power, but also suppresses the vibration better than without the time delay or with delay parameters chosen from the SPS region. In addition, as shown in Table 1, for any selected values of WF_1, the parameters $k_1 = 4$, $\tau = 0.4131$ and $d_0 = 15$ mm lead to the best perfection rate.

Table 1 Best values for d_0 to have maximum perfection rate.

Delay parameters	d_0(mm)	PR(%)		
		$WF_1 = 0.2$	$WF_1 = 0.5$	$WF_1 = 0.8$
Without delay ($k_1 = 0$)	15	55.1408	51.2454	47.3501
	20	55.1359	51.2333	47.3307
	25	55.1353	51.2317	47.3281
$k_1 = 4$, $\tau = 0.4131$	15	**55.1429**	**51.2508**	**47.3586**
	20	55.1353	51.2317	47.3282
	25	55.1353	51.2317	47.3281
$k_1 = 4$, $\tau = 0.75$	15	55.1375	51.2372	47.3363
	20	55.1363	51.2341	47.3320
	25	55.1373	51.2366	47.3360

Figure 7 shows the influence of the time delay parameters on the output power for different values of the excitation frequencies while varying the external load resistance for different delay parameters chosen from the SPS and MPS regions and without delay. The excitation frequency and time delay parameters can significantly influence the output power. The maximum output power occurs at optimum external load resistances of $2.7\,\mathrm{k\Omega}$, $10.34\,\mathrm{k\Omega}$ and $7.8\,\mathrm{k\Omega}$ for the excitation frequencies of $\Omega/\omega = 0.46$, $\Omega/\omega = 1.46$ and $\Omega/\omega = 1$, respectively, for any values of the delay parameters. The maximum scavenged power occurs at $\Omega/\omega = 1$ and is equal to

24.1μW, 70μW and 55μW for the delay parameters of $k_1 = 4$, $\tau = 0.75$ and $k_1 = 4$ and $\tau = 0.4131$ and without delay, respectively. It can be concluded that choosing delay parameters from the MPS region can increase the output power without changing the optimum load resistance.

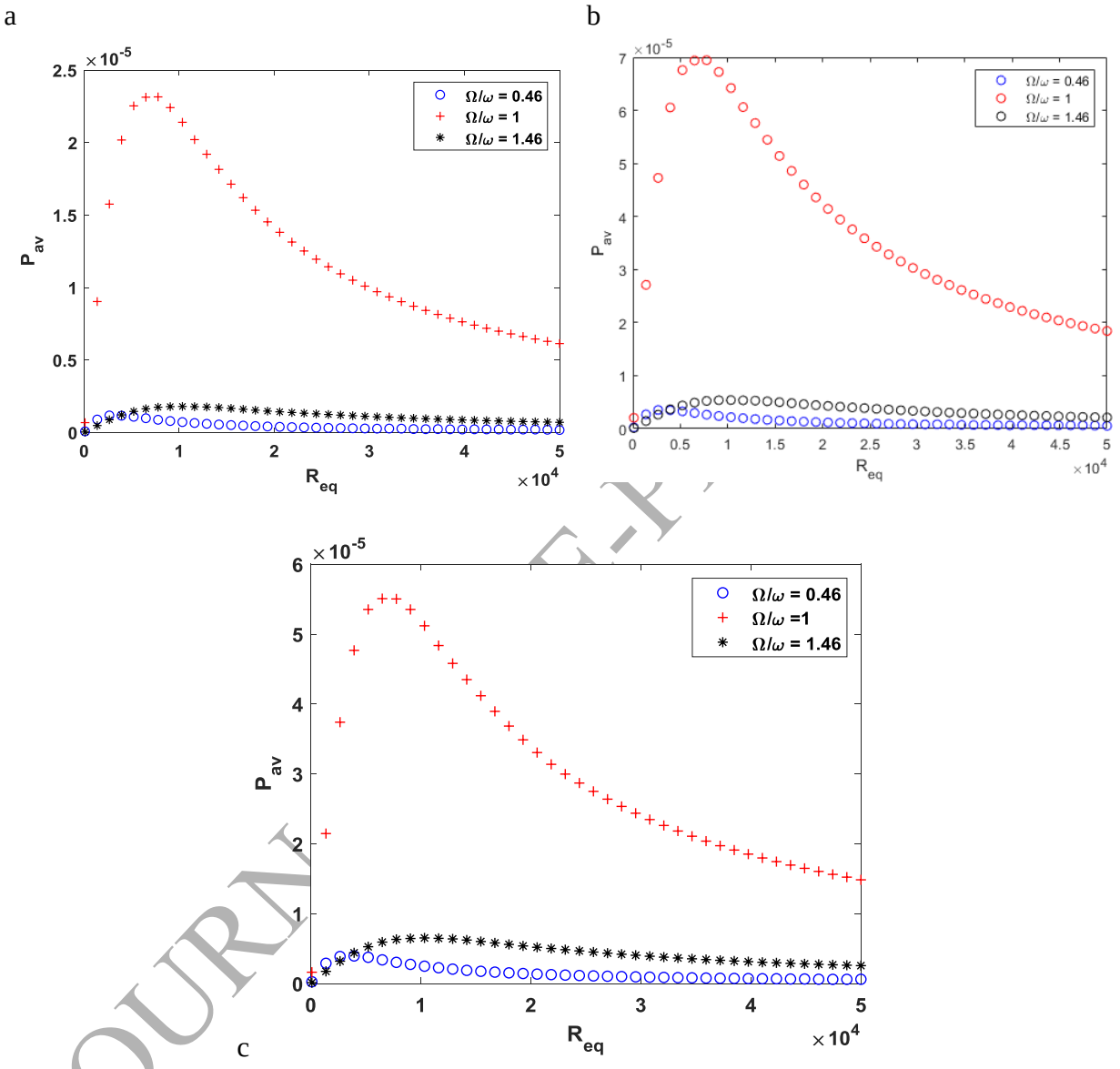

Fig. 7 Variation of the average output power versus load resistance for **(a)** $k_1 = 4$ and $\tau = 0.75$ **(b)** $k_1 = 4$ and $\tau = 0.4131$ and **(c)** without time delay.

Figure 8 illustrates the effect of the cubic nonlinear parameter of the exerted force between magnets (β) on the frequency response of the vibration and power amplitudes. The figure highlights the importance of the nonlinearity as opposed to a linear characteristic and shows

results for $k_1 = 4$, $\tau = 0.4131$, $d_0 = 19.53\text{mm}$, $R_{eq} = 188\text{M}\Omega$. It is seen that the frequency response curves for $\beta \neq 0$ are bent to the right, which depicts a hardening behavior. In addition, there exists three equilibria, two of which are stable and the other one is unstable. Also, due to the existence of the stable and unstable manifolds in the multi-valued frequency response curves, bifurcation occurs in the system. The stable branches meet the unstable branch at the fold bifurcation points A, B, C, D, and E. Furthermore, when the nonlinear model is excited by forward and backward frequency sweeping, the result is the nonlinear behaviors of jumps and hysteresis. The influence of β on the frequency response of the system is significant and this parameter remarkably alters the locus of bifurcation points and the hysteresis region.

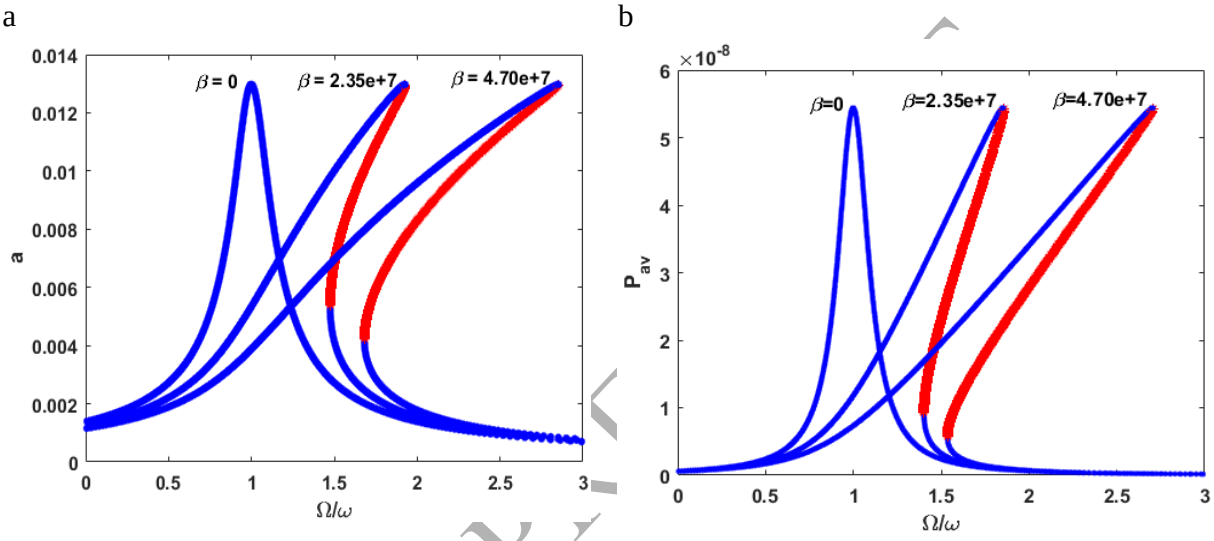

Fig. 8 Influence of the nonlinear parameter β of the exerted force between magnets on the **(a)** vibration and **(b)** power amplitudes for $k_1 = 4$, $\tau = 0.4131$, $d_0 = 19.53$, $R_{eq} = 188\text{M}\Omega$.

Figure 9 shows the influence of the excitation amplitude on the vibration and power amplitudes for different values of the time delay parameters chosen from the SPS and MPS regions. For each value of the time delay parameters, increasing the excitation amplitude results in a rise in the vibration and power amplitudes monotonically. High excitation amplitudes result in an extended range of large amplitude responses that are obtained by engaging the nonlinearity of the system. Also, for the excitation amplitude of $F_1 = 5\,\text{m/s}^2$, and for the time delay parameters selected as $k_1 = 4$ and $\tau = 0.4131$, the system is capable of harvesting more energy over a broad range of excitation frequencies, in contrast to the time delay parameters chosen as $k_1 = 4$ and $\tau = 0.75$. Thus, the system with time delay parameters chosen from the MPS region is capable of engaging nonlinearities and relocates the peak resonance away from linear resonance. Thus, for this case, the ability to tune the restoring forces becomes an essential consideration for applications with either fixed or varying excitations.

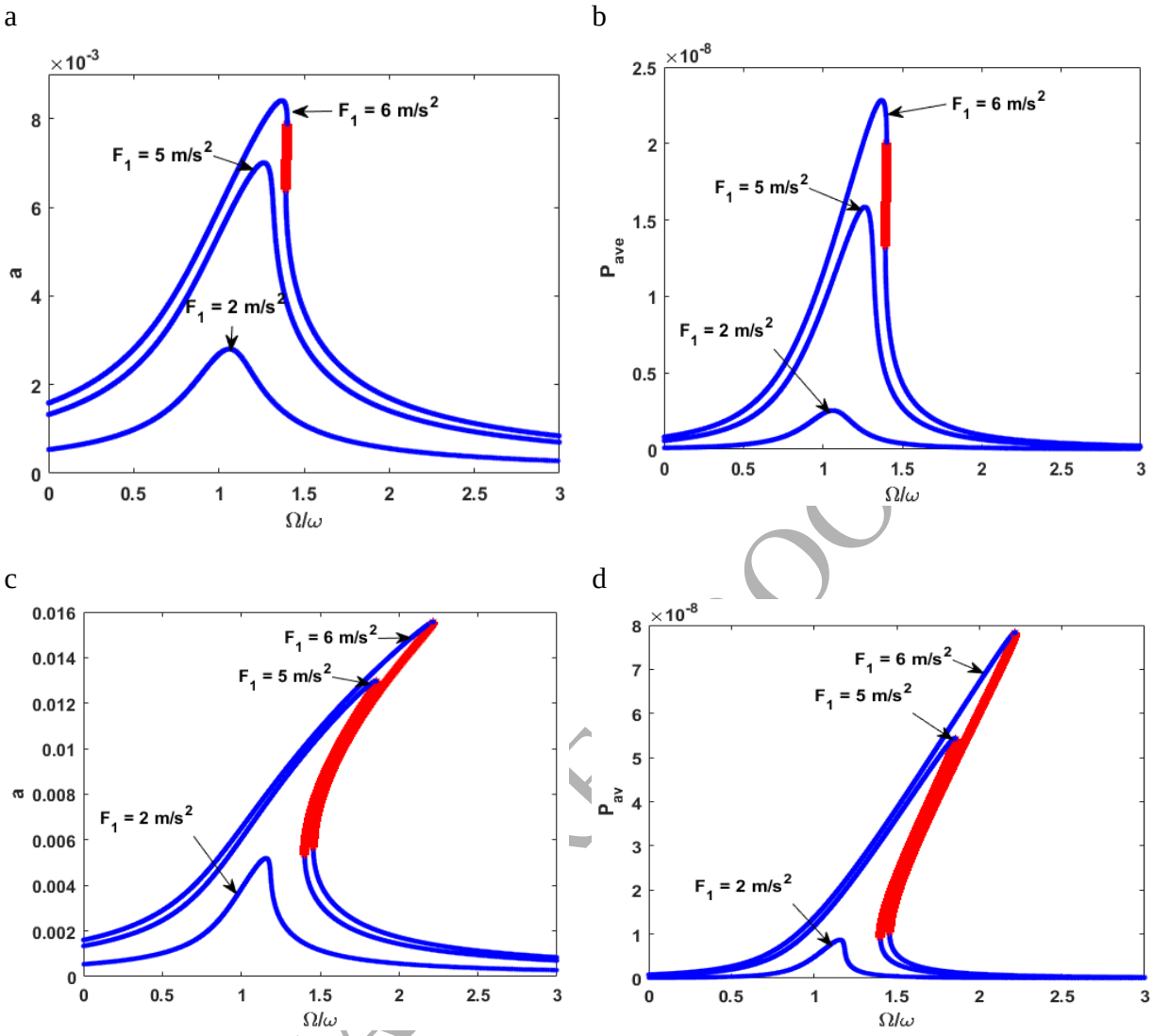

Fig. 9 Vibration and power amplitudes for different values of the excitation amplitude for **(a,b)** $k_1 = 4$ and $\tau = 0.75$ **(c,d)** $k_1 = 4$ and $\tau = 0.4131$.

Figure 10 investigates the influence of the time delay gain k_1 on the vibration amplitude as the base excitation amplitude is selected from two different points in the SPS and MPS regions, and the other parameters are arbitrarily selected as $\frac{\Omega}{\omega} = 1$, $R_{eq} = 0.5\text{k}\Omega$ and $d_0 = 19.53\text{mm}$. The vibration amplitude increases as the base excitation amplitude is increased and there exists only one stable solution regardless of the excitation amplitude. For the SPS region, Fig. 10(b), the biggest vibration amplitude occurs at the smallest k_1. Thus, the time delay suppresses the vibration. A different scenario happens for the points selected in the MPS regions, shown in Fig. 10(a). For a delay gain of $0 \leq k_1 \leq 4$, the largest vibration amplitude occurs at the largest value of the delay gain k_1. This means that if $k_1 < k_{cr}$ the external force acts like an actuator that

additionally stimulates vibrations and when k_1 crosses k_{cr} the solution loses its stability. However, as we continue to increase the delay gain it is observed that the control feedback again suppresses the vibration amplitude, as explained for the Fig. 10(b) case.

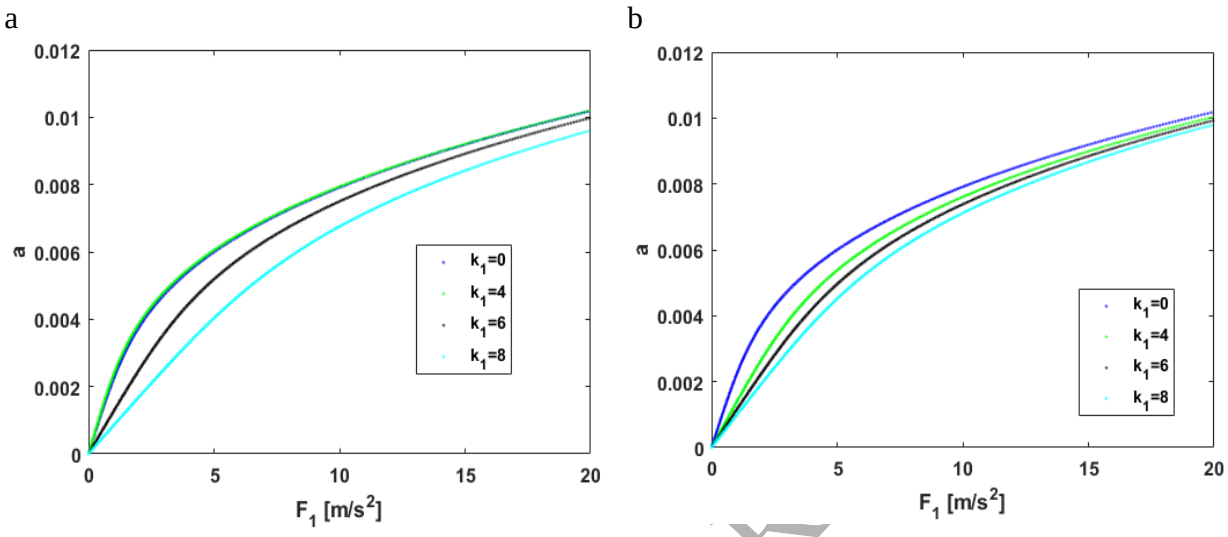

Fig.10 Influence of the time delay gain k_1 on the vibration amplitude versus base excitation amplitude for (a) time delay $\tau = 0.4131$ chosen from the MPS region and (b) time delay $\tau = 0.75$ chosen from the SPS region, for $\frac{\Omega}{\omega} = 1, R_{eq} = 0.5\text{k}\Omega$ and $d_0 = 19.53\text{mm}$.

A similar example to Fig. 10, for a different excitation frequency of $\frac{\Omega}{\omega} = 1.42$, is shown in Fig. 11. It is seen that for some values of the delay gains chosen from the MPS (Fig. 11(a)) and SPS (Fig. 11(b)) regions there exist two stable and one unstable solutions, whereas for some other delay gains there exist only one stable solution. For example, with the delay gain $k_1 = 4$ and for both the SPS and MPS regions, a force sweep leads to jumps and hysteresis in the response. For $k_1 = 8$ and for both the SPS and MPS regions, there just exists one stable nontrivial solution for the system. For these cases, the delay gain increases the response monotonically as F_1 increases and neither a jump nor a hysteresis occurs in the system. In addition, when the delay gain is equal to $k_1 = 6$, it is seen that for the point chosen from the MPS region there exists two stable and one unstable solutions, whereas for the point chosen from the SPS region there exists only one stable solution.

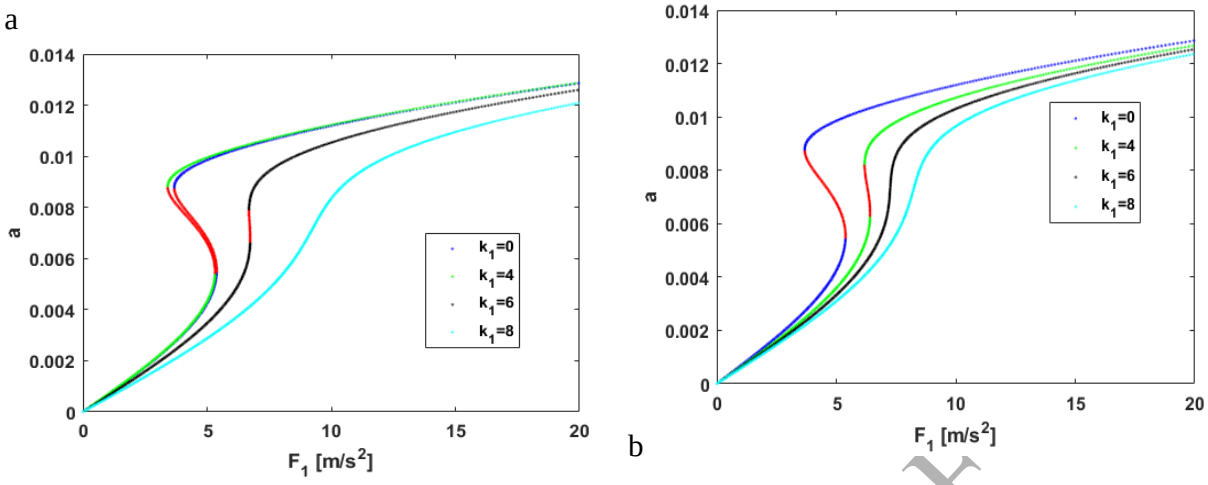

Fig.11 Influence of the time delay amplitude k_1 on the vibrations amplitude versus base excitation amplitude for (a) time delay $\tau = 0.4131$ chosen from the MPS region and (b) time delay $\tau = 0.75$ chosen from the SPS region, for $\frac{\Omega}{\omega} = 1.42, R_{eq} = 0.5\text{k}\Omega$ and $d_0 = 19.53\text{mm}$.

Conclusions

In the presented paper, time delay in a nonlinear magnetic levitation system is introduced for both energy harvesting and vibration suppression. To study the influence of the time delay on the vibration and power amplitude, we plotted the stability map of the system in the domain of the delay parameters. The results show there are two kinds of responses: Single Periodic Solution (SPS) and Multiple Periodic Solution (MPS). Next, we choose different points from the SPS and MPS regions to study the effect of the introduced time delay on the vibration and power amplitudes. It was observed that the points chosen from the MPS region results in more power generated over a broad range of excitation frequencies. Also, for the points chosen from the MPS region, increasing the delay gain first increases the vibration and power and then decreases it. This means that there is an optimum value for the delay gain. In contrast, for a point chosen from the SPS region, it was shown that increasing the delay gain decreases the vibration and power monotonically. Furthermore, the influence of the distance between the magnets on the frequency responses of the vibration and power amplitudes was studied. It was shown that, without the time delay, increasing the distance between the magnets increases the output power and also extends the frequency range where more power could be scavenged. However, with the time delay and for a point chosen from the SPS region, it was shown that the maximum vibration does not necessarily occur simultaneously with the maximum power. It was shown that increasing the distance between the magnets increases the vibration amplitude and decreases the output power. Also, to design the optimum system with the maximum power and minimum vibration the so-called Perfection Rate (PR) was introduced. The effect of the distance between the magnets on the PR for different values of the time delay parameters was studied. The optimum values for the time delay parameters and the distance between magnets were calculated in a way to have the

maximum value for the PR. The effect of the external resistance load on the output power was studied. It was shown that there is an optimum external load resistance to generate the maximum output power and the optimum values were given.

Appendix A

$$C_1 = \mu + \frac{\gamma_1\gamma_2\gamma_3}{2({\gamma_2}^2 + \omega^2)} + \frac{1}{2\omega}k_1 \sin(\omega\tau) \tag{56}$$

$$C_2 = -\sigma + \frac{3\beta {F_0}^2}{2\omega^5} + \frac{\gamma_1\gamma_3\omega}{2({\gamma_2}^2 + \omega^2)} - \frac{1}{2\omega}k_1 \cos(\omega\tau) \tag{57}$$

$$C_3 = \frac{3\beta}{8\omega} \tag{58}$$

References

[1] M. Penella and M. Gasulla, "A review of commercial energy harvesters for autonomous sensors," in *Instrumentation and Measurement Technology Conference Proceedings, 2007. IMTC 2007. IEEE*, 2007, pp. 1-5.

[2] J. A. Paradiso and T. Starner, "Energy scavenging for mobile and wireless electronics," *IEEE Pervasive computing*, pp. 18-27, 2005.

[3] R. Harne, A. Sun, and K. Wang, "Leveraging nonlinear saturation-based phenomena in an L-shaped vibration energy harvesting system," *Journal of Sound and Vibration*, vol. 363, pp. 517-531, 2016.

[4] L. Wang and F. Yuan, "Vibration energy harvesting by magnetostrictive material," *Smart Materials and Structures*, vol. 17, p. 045009, 2008.

[5] N. Tran, M. H. Ghayesh, and M. Arjomandi, "Ambient vibration energy harvesters: A review on nonlinear techniques for performance enhancement," *International Journal of Engineering Science*, vol. 127, pp. 162-185, 2018.

[6] D. P. Arnold, "Review of microscale magnetic power generation," *IEEE Transactions on Magnetics*, vol. 43, pp. 3940-3951, 2007.

[7] N. G. Elvin and A. A. Elvin, "An experimentally validated electromagnetic energy harvester," *Journal of Sound and Vibration*, vol. 330, pp. 2314-2324, 2011.

[8] S. Meninger, J. O. Mur-Miranda, R. Amirtharajah, A. Chandrakasan, and J. H. Lang, "Vibration-to-electric energy conversion," *IEEE Transactions on Very Large Scale Integration (VLSI) Systems*, vol. 9, pp. 64-76, 2001.

[9] L. G. W. Tvedt, D. S. Nguyen, and E. Halvorsen, "Nonlinear behavior of an electrostatic energy harvester under wide-and narrowband excitation," *Journal of Microelectromechanical systems*, vol. 19, pp. 305-316, 2010.

[10] X. Xie and Q. Wang, "A mathematical model for piezoelectric ring energy harvesting technology from vehicle tires," *International Journal of Engineering Science*, vol. 94, pp. 113-127, 2015.

[11] X. Xie, Q. Wang, and N. Wu, "Energy harvesting from transverse ocean waves by a piezoelectric plate," *International Journal of Engineering Science*, vol. 81, pp. 41-48, 2014.

[12] M. Rezaei, S. E. Khadem, and P. Firoozy, "Broadband and tunable PZT energy harvesting utilizing local nonlinearity and tip mass effects," *International Journal of Engineering Science*, vol. 118, pp. 1-15, 2017.
[13] X. Xie, Q. Wang, and N. Wu, "A ring piezoelectric energy harvester excited by magnetic forces," *International Journal of Engineering Science*, vol. 77, pp. 71-78, 2014.
[14] A. Adly, D. Davino, A. Giustiniani, and C. Visone, "Experimental tests of a magnetostrictive energy harvesting device toward its modeling," *Journal of Applied Physics*, vol. 107, p. 09A935, 2010.
[15] B. Mann and N. Sims, "Energy harvesting from the nonlinear oscillations of magnetic levitation," *Journal of Sound and Vibration*, vol. 319, pp. 515-530, 2009.
[16] S. Jiang, X. Li, S. Guo, Y. Hu, J. Yang, and Q. Jiang, "Performance of a piezoelectric bimorph for scavenging vibration energy," *Smart Materials and Structures*, vol. 14, p. 769, 2005.
[17] Y. Hu, H. Xue, and H. Hu, "A piezoelectric power harvester with adjustable frequency through axial preloads," *Smart materials and structures*, vol. 16, p. 1961, 2007.
[18] H. Hu, Z. Cui, and J. Cao, "Performance of a piezoelectric bimorph harvester with variable width," *Journal of Mechanics*, vol. 23, pp. 197-202, 2007.
[19] P. Firoozy, S. E. Khadem, and S. M. Pourkiaee, "Power enhancement of broadband piezoelectric energy harvesting using a proof mass and nonlinearities in curvature and inertia," *International Journal of Mechanical Sciences*, vol. 133, pp. 227-239, 2017.
[20] P. Firoozy, S. E. Khadem, and S. M. Pourkiaee, "Broadband energy harvesting using nonlinear vibrations of a magnetopiezoelastic cantilever beam," *International Journal of Engineering Science*, vol. 111, pp. 113-133, 2017.
[21] L. Tang, Y. Yang, and C. K. Soh, "Toward broadband vibration-based energy harvesting," *Journal of intelligent material systems and structures*, vol. 21, pp. 1867-1897, 2010.
[22] H. Wu, L. Tang, Y. Yang, and C. K. Soh, "Development of a broadband nonlinear two-degree-of-freedom piezoelectric energy harvester," *Journal of Intelligent Material Systems and Structures*, vol. 25, pp. 1875-1889, 2014.
[23] A. Abdelkefi and N. Barsallo, "Comparative modeling of low-frequency piezomagnetoelastic energy harvesters," *Journal of Intelligent Material Systems and Structures*, vol. 25, pp. 1771-1785, 2014.
[24] D. A. Barton, S. G. Burrow, and L. R. Clare, "Energy harvesting from vibrations with a nonlinear oscillator," *Journal of Vibration and Acoustics*, vol. 132, p. 021009, 2010.
[25] M. F. Daqaq, "Response of uni-modal duffing-type harvesters to random forced excitations," *Journal of Sound and Vibration*, vol. 329, pp. 3621-3631, 2010.
[26] S. C. Stanton, C. C. McGehee, and B. P. Mann, "Reversible hysteresis for broadband magnetopiezoelastic energy harvesting," *Applied Physics Letters*, vol. 95, p. 174103, 2009.
[27] C. Lan, L. Tang, W. Qin, and L. Xiong, "Magnetically coupled dual-beam energy harvester: Benefit and trade-off," *Journal of Intelligent Material Systems and Structures*, vol. 29, pp. 1216-1235, 2018.
[28] R. Harne and K. Wang, "A review of the recent research on vibration energy harvesting via bistable systems," *Smart materials and structures*, vol. 22, p. 023001, 2013.
[29] Z. Wu, R. L. Harne, and K.-W. Wang, "Energy harvester synthesis via coupled linear-bistable system with multistable dynamics," *Journal of Applied Mechanics*, vol. 81, p. 061005, 2014.
[30] R. L. Harne and K.-W. Wang, *Harnessing bistable structural dynamics: for vibration control, energy harvesting and sensing*: John Wiley & Sons, 2017.
[31] J. Cao, S. Zhou, D. J. Inman, and Y. Chen, "Chaos in the fractionally damped broadband piezoelectric energy generator," *Nonlinear Dynamics*, vol. 80, pp. 1705-1719, 2015.
[32] A. Erturk and D. J. Inman, "Broadband piezoelectric power generation on high-energy orbits of the bistable Duffing oscillator with electromechanical coupling," *Journal of Sound and Vibration*, vol. 330, pp. 2339-2353, 2011.

[33] S. C. Stanton, C. C. McGehee, and B. P. Mann, "Nonlinear dynamics for broadband energy harvesting: Investigation of a bistable piezoelectric inertial generator," *Physica D: Nonlinear Phenomena*, vol. 239, pp. 640-653, 2010.
[34] S. Zhou, J. Cao, D. J. Inman, J. Lin, S. Liu, and Z. Wang, "Broadband tristable energy harvester: modeling and experiment verification," *Applied Energy*, vol. 133, pp. 33-39, 2014.
[35] J. Cao, S. Zhou, W. Wang, and J. Lin, "Influence of potential well depth on nonlinear tristable energy harvesting," *Applied Physics Letters*, vol. 106, p. 173903, 2015.
[36] P. Kim and J. Seok, "A multi-stable energy harvester: dynamic modeling and bifurcation analysis," *Journal of Sound and Vibration*, vol. 333, pp. 5525-5547, 2014.
[37] L. Tang and Y. Yang, "A nonlinear piezoelectric energy harvester with magnetic oscillator," *Applied Physics Letters*, vol. 101, p. 094102, 2012.
[38] Y. Liu and S. Zhao, "Controllability for a class of linear time-varying impulsive systems with time delay in control input," *IEEE Transactions on Automatic Control*, vol. 56, pp. 395-399, 2010.
[39] H. Du and N. Zhang, "H∞ control for buildings with time delay in control via linear matrix inequalities and genetic algorithms," *Engineering Structures*, vol. 30, pp. 81-92, 2008.
[40] X. Sun, J. Xu, and J. Fu, "The effect and design of time delay in feedback control for a nonlinear isolation system," *Mechanical Systems and Signal Processing*, vol. 87, pp. 206-217, 2017.
[41] X. Sun, S. Zhang, and J. Xu, "Parameter design of a multi-delayed isolator with asymmetrical nonlinearity," *International Journal of Mechanical Sciences*, vol. 138, pp. 398-408, 2018.
[42] X. Sun, F. Wang, and J. Xu, "Dynamics and realization of a feedback-controlled nonlinear isolator with variable time delay," *Journal of Vibration and Acoustics*, vol. 141, p. 021005, 2019.
[43] C. Cheng, S. Li, Y. Wang, and X. Jiang, "On the analysis of a high-static-low-dynamic stiffness vibration isolator with time-delayed cubic displacement feedback," *Journal of Sound and Vibration*, vol. 378, pp. 76-91, 2016.
[44] J. Liu and K. Liu, "A tunable electromagnetic vibration absorber: Characterization and application," *Journal of Sound and Vibration*, vol. 295, pp. 708-724, 2006.
[45] J. Liu and K. Liu, "Application of an active electromagnetic vibration absorber in vibration suppression," *Structural Control and Health Monitoring: The Official Journal of the International Association for Structural Control and Monitoring and of the European Association for the Control of Structures*, vol. 17, pp. 278-300, 2010.
[46] Y. Zhao and J. Xu, "Using the delayed feedback control and saturation control to suppress the vibration of the dynamical system," *Nonlinear Dynamics*, vol. 67, pp. 735-753, 2012.
[47] F. Wang and J. Xu, "Parameter design for a vibration absorber with time-delayed feedback control," *Acta Mechanica Sinica*, pp. 1-17, 2018.
[48] M. Belhaq and M. Hamdi, "Energy harvesting from quasi-periodic vibrations," *Nonlinear Dynamics*, vol. 86, pp. 2193-2205, 2016.
[49] Z. Ghouli, M. Hamdi, F. Lakrad, and M. Belhaq, "Quasiperiodic energy harvesting in a forced and delayed Duffing harvester device," *Journal of Sound and Vibration*, vol. 407, pp. 271-285, 2017.
[50] Z. Ghouli, M. Hamdi, and M. Belhaq, "Energy harvesting from quasi-periodic vibrations using electromagnetic coupling with delay," *Nonlinear Dynamics*, vol. 89, pp. 1625-1636, 2017.
[51] T. Kalmár-Nagy, G. Stépán, and F. C. Moon, "Subcritical Hopf bifurcation in the delay equation model for machine tool vibrations," *Nonlinear Dynamics*, vol. 26, pp. 121-142, 2001.
[52] G. Stépán, R. Szalai, and T. Insperger, "Nonlinear dynamics of high-speed milling subjected to regenerative effect," ed: Wiley VCH, Weinheim, 2004, pp. 111-128.
[53] R. Rusinek, A. Weremczuk, and J. Warminski, "Regenerative model of cutting process with nonlinear duffing oscillator," *Mechanics and Mechanical Engineering*, vol. 15, pp. 129-143, 2011.

[54] A. S. Kammer and N. Olgac, "Delayed feedback control scheme for improved energy harvesting using piezoelectric networks," *Journal of Intelligent Material Systems and Structures*, vol. 29, pp. 1546-1559, 2018.
[55] A. S. Kammer and N. Olgac, "Delayed-feedback vibration absorbers to enhance energy harvesting," *Journal of Sound and Vibration*, vol. 363, pp. 54-67, 2016.
[56] K. W. Yung, P. B. Landecker, and D. D. Villani, "An analytic solution for the force between two magnetic dipoles," *Physical Separation in Science and Engineering*, vol. 9, pp. 39-52, 1998.
[57] A. Nayfeh and D. Mook, "Nonlinear Oscillations, Wiley, New York, 1979," *MATH Google Scholar*.
[58] R. Rusinek, A. Weremczuk, K. Kecik, and J. Warminski, "Dynamics of a time delayed Duffing oscillator," *International Journal of Non-Linear Mechanics*, vol. 65, pp. 98-106, 2014.
[59] H. Zoka and A. Afsharfard, "Double stiffness vibration suppressor and energy harvester: An experimental study," *Mechanical Systems and Signal Processing*, vol. 121, pp. 1-13, 2019.
[60] A. Afsharfard and A. Farshidianfar, "Application of single unit impact dampers to harvest energy and suppress vibrations," *Journal of Intelligent Material Systems and Structures*, vol. 25, pp. 1850-1860, 2014.

GRAPHICAL ABSTRACT